applied optics

Dual-output filter-free microwave photonic single sideband up-converter with high mixing spur suppression

Jiewen Ding,[1] Dan Zhu,[1,2] Bowen Zhang,[1] and Shilong Pan[1,3]

[1]College of Electronic and Information Engineering, Nanjing University of Aeronautics and Astronautics, Nanjing 210016, China
[2]e-mail: danzhu@nuaa.edu.cn
[3]e-mail: pans@nuaa.edu.cn

Received 17 May 2021; revised 20 July 2021; accepted 3 August 2021; posted 6 August 2021 (Doc. ID 431196); published 2 September 2021

A dual-output filter-free microwave photonic single sideband (SSB) up-converter with the mixing spurs highly suppressed is proposed and experimentally demonstrated. By introducing the balanced Hartley structure using a 90° optical hybrid, the lower sideband (LSB) and upper sideband (USB) up-converted RF signals can be generated simultaneously and output separately, with no need of either optical or electrical filtering. The structure avoids the special requirement with the optical modulation format of the local oscillator (LO) signal. The intermediate frequency signal is modulated with the optical carrier suppressed -SSB modulation format. The undesired optical components are highly suppressed. In this way, the high sideband and LO leakage suppression ratios of the SSB up-converter are guaranteed. The dual-output SSB up-conversion is experimentally achieved within the working frequency range of 10–30 GHz. The undesired sideband and LO leakage suppression ratios are larger than 67 dB for the whole frequency range. The spurious-free dynamic range of larger than 95.6 dBc · Hz$^{2/3}$ has also been achieved experimentally for both the LSB and USB up-conversion conditions.

https://doi.org/10.1364/AO.431196

1. INTRODUCTION

Frequency up-conversion is a key function in modern radio frequency (RF) systems, such as radar, wireless communication, electronic warfare, and cognitive radio systems [1–3]. Typically, the double sideband (DSB) up-converters generate both the upper sideband (USB) RF signal at $f_{\mathrm{USB}} = f_{\mathrm{LO}} + f_{\mathrm{IF}}$ and the lower sideband (LSB) RF signal at $f_{\mathrm{LSB}} = f_{\mathrm{LO}} - f_{\mathrm{IF}}$, where f_{LO} and f_{IF} are the frequencies of the local oscillator (LO) signal and the intermediate frequency (IF) signal, respectively. Meanwhile, the single sideband (SSB) up-converters only generate the USB or LSB RF signal, which have significant advantages of improved spectrum efficiency. It is important for future RF applications to achieve multi-functions with limited spectrum sources [4,5]. One key characteristic with the SSB up-converters is the sideband suppression ratio, referring to the power difference between the desired up-converted RF sideband and the undesired one. Another key characteristic is the LO leakage suppression ratio, referring to the power difference between the desired up-converted RF sideband and the LO leakage. The frequencies of the undesired up-converted RF signal sideband and the LO leakage are very close to the wanted RF signal. Thus, high sideband and LO leakage suppression ratios are required to guarantee the RF system performances [6–9]. In addition, the urgent demand for a wide working frequency range is also created with the SSB up-converters.

Recently, microwave photonic SSB up-converters have been widely researched, due to the advantages of large working bandwidth, high isolation, and electromagnetic interference immunity (EMI), brought on by photonics [10,11]. Two typical methods have been proposed to achieve the microwave photonic SSB up-converters. One method is to use microwave photonic mixing to achieve the DSB up-conversion and remove the undesired up-converted RF sideband by using electrical filters [12]. Electrical filters with high center frequency, high out-of-band suppression ratio, sharp edge roll-off, and wide tuning range are needed, which are hard to achieve. Another method is based on the optical carrier suppressed SSB (CS-SSB) modulation of the IF/LO signals, generating only the +1st or −1 st-order optical sidebands. After photodetection, a USB or LSB RF signal will be generated. To achieve the optical CS-SSB modulation with both the IF/LO signals, one way is using optical filters to remove the undesired optical sideband components [13–17]. Strict requirements are needed with the optical filters, in the respects of the high out-of-band suppression ratio and the sharp edge roll-off, which are difficult to realize. To avoid the optical filters, the other way is to use dual-parallel Mach–Zehnder modulators (DPMZMs) [18] or in-phase and quadrature (I/Q) modulators [19,20] to achieve the optical CS-SSB modulation. For this condition, the sideband suppression ratio and the LO leakage suppression ratio are limited by the extinction ratio of the used modulators, with the experimentally achieved values of about 30–40 dB [18–20]. Therefore, the filter-free microwave photonic SSB up-converters with high sideband and LO leakage suppression ratios are urgently desired.

In this work, a filter-free microwave photonic SSB up-converter with high sideband and LO leakage suppression ratios is proposed and demonstrated. (1) Based on the balanced Hartley structure using a 90° optical hybrid, the up-converted USB and LSB RF signals can be generated simultaneously and output separately, with no need of either optical or electrical filtering. (2) The structure only requires the optical CS-SSB modulation format with the IF signal, avoiding the special requirement with the optical modulation format of the LO signal. The undesired sideband and the LO leakage suppression ratios of the SSB up-converter are determined by the undesired optical components suppression ratio of the optical CS-SSB modulated IF signal. A proof-of-concept is taken. To achieve high sideband suppression ratio and LO leakage suppression ratio, an acousto-optic modulator (AOM) is introduced to modulate the IF signal. An MZM is used to modulate the LO signal, guaranteeing the wide working frequency range of the LO signal. In this way, the filter-free dual-output microwave photonic SSB up-converter is achieved with high mixing spur suppression ratio. Dual-output SSB up-conversion is achieved within the working frequency range of 10–30 GHz. For the whole working frequency range, the suppression ratios with the undesired sideband and the LO leakage are larger than 67 dB.

2. PRINCIPLE

Figure 1 shows the structure of the proposed dual-output filter-free microwave photonic SSB up-converter. The optical carrier with the angular frequency of ω_c is generated from a laser diode (LD) and split into two parts. One part injects into an AOM, at which the IF signal $S_{\mathrm{IF}}(t)=\cos(\omega_{\mathrm{IF}}t+\theta_{\mathrm{IF}})$ is modulated with the optical CS-SSB. The other part injects into the Mach–Zehnder modulator (MZM), at which the LO signal $S_{\mathrm{LO}}(t)=\cos(\omega_{\mathrm{LO}}t+\theta_{\mathrm{LO}})$ is modulated with the optical carrier suppressed DSB (CS-DSB) modulation format. The optical signals output from the AOM and the MZM are expressed as follows:

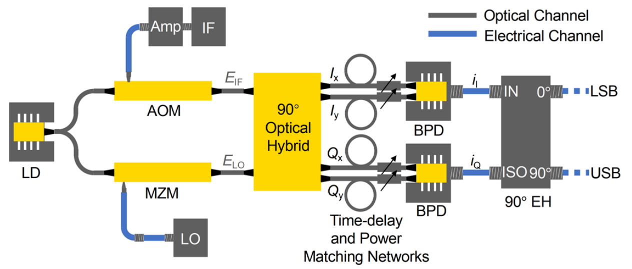

Fig. 1. Schematic diagram of the proposed filter-free microwave photonic SSB up-converter structure. LD, laser diode; Amp, power amplifier; BPD, balanced photodetector; 90° EH, 90° electrical hybrid.

$$\begin{cases} E_{\mathrm{IF}}(t)\propto A_{-1}\exp[j(\omega_c t-\omega_{\mathrm{IF}}t-\theta_{\mathrm{IF}})]+A_0\exp(j\omega_c t) \\ \qquad +A_1\exp[j(\omega_c t+\omega_{\mathrm{IF}}t+\theta_{\mathrm{IF}})] \\ E_{\mathrm{LO}}(t)\propto \sum\limits_{n=0}^{+\infty} B_n J_n(\beta)\exp[j(\omega_c t\pm n\omega_{\mathrm{LO}}t\pm n\theta_{\mathrm{LO}})] \end{cases}, \quad (1)$$

where A_0, A_1, and A_{-1} are the amplitudes of the optical carrier and the ± 1 st-order optical sideband for the AOM output, B_n is the amplitudes of the optical carrier ($n=0$), and the nth-order optical sidebands ($n\neq 0$) for the MZM output, respectively. $J_n(\cdot)$ is the nth-order Bessel function of the first kind, and β is the modulation index at the MZM. It should be noted that either positive or negative frequency shift can be realized by AOM [21], and both of them can be used in this structure. In this paper, the positive frequency shift is taken for analyses. The outputs from the AOM and the MZM are injected into the optical signal port and the optical LO port of the 90° optical hybrid, respectively. The 90° optical hybrid outputs two in-phase (I_x,I_y) and two orthogonal (Q_x,Q_y) optical signals as follows:

$$\begin{bmatrix} I_x \\ I_y \\ Q_x \\ Q_y \end{bmatrix} = \begin{bmatrix} 1 & +1 \\ 1 & -1 \\ 1 & +j \\ 1 & -j \end{bmatrix} \begin{bmatrix} E_{\mathrm{IF}} \\ E_{\mathrm{LO}} \end{bmatrix} = \begin{bmatrix} E_{\mathrm{IF}}+E_{\mathrm{LO}} \\ E_{\mathrm{IF}}-E_{\mathrm{LO}} \\ E_{\mathrm{IF}}+jE_{\mathrm{LO}} \\ E_{\mathrm{IF}}-jE_{\mathrm{LO}} \end{bmatrix}. \quad (2)$$

The optical signals are sent into two balanced photodetectors (BPDs), respectively, with the electrical outputs as follows:

$$\begin{cases} i_{\mathrm{I}}(t)=\Re_1(I_x I_x^*-I_y I_y^*) \\ \propto 2\Re_1\sum\limits_{n=0}^{+\infty} B_n J_n(\beta)\,[(A_{-1}+A_1)\cos(-\omega_{\mathrm{IF}}t-\theta_{\mathrm{IF}}+n\omega_{\mathrm{LO}}t+n\theta_{\mathrm{LO}}) \\ +(A_0+A_0)\cos(n\omega_{\mathrm{LO}}t+n\theta_{\mathrm{LO}}) \\ +(A_{-1}+A_1)\cos(\omega_{\mathrm{IF}}t+\theta_{\mathrm{IF}}+n\omega_{\mathrm{LO}}t+n\theta_{\mathrm{LO}})] \\ i_{\mathrm{Q}}(t)=\Re_2(Q_x Q_x^*-Q_y Q_y^*) \\ \propto 2\Re_2\sum\limits_{n=0}^{+\infty} B_n J_n(\beta)\,[(A_{-1}-A_1)\sin(-\omega_{\mathrm{IF}}t-\theta_{\mathrm{IF}}+n\omega_{\mathrm{LO}}t+n\theta_{\mathrm{LO}}) \\ +(A_0-A_0)\sin(n\omega_{\mathrm{LO}}t+n\theta_{\mathrm{LO}}) \\ +(-A_{-1}+A_1)\sin(\omega_{\mathrm{IF}}t+\theta_{\mathrm{IF}}+n\omega_{\mathrm{LO}}t+n\theta_{\mathrm{LO}})] \end{cases}, \quad (3)$$

where $\Re_1$, $\Re_2$ are the responsivities of the two BPDs, respectively. A pair of phase orthogonal electrical signals is generated. The two electrical signals are combined through a 90° electrical hybrid, and the RF signals are generated from the two output ports of the 90° electrical hybrid, which are as follows:

$$\begin{cases} i_1(t) = i_{\mathrm{I}}(t) + i_{\mathrm{Q}}(t)\angle 90^\circ \propto 2\sum_{n=0}^{+\infty} B_n J_n(\beta)\,[A_{-1}(\Re_1+\Re_2)\cos(-\omega_{\mathrm{IF}}t - \theta_{\mathrm{IF}} + n\omega_{\mathrm{LO}}t + n\theta_{\mathrm{LO}}) \\ +2\Re_1 A_0 \cos(n\omega_{\mathrm{LO}}t + n\theta_{\mathrm{LO}}) + A_1(\Re_1+\Re_2)\cos(\omega_{\mathrm{IF}}t + \theta_{\mathrm{IF}} + n\omega_{\mathrm{LO}}t + n\theta_{\mathrm{LO}})] \text{ when } \quad \Re_1 \approx \Re_2 \\ i_2(t) = i_{\mathrm{I}}(t)\angle 90^\circ + i_{\mathrm{Q}}(t) \\ \propto 2\sum_{n=0}^{+\infty} B_n J_n(\beta)\,[-A_1(\Re_1+\Re_2)\sin(-\omega_{\mathrm{IF}}t - \theta_{\mathrm{IF}} + n\omega_{\mathrm{LO}}t + n\theta_{\mathrm{LO}}) - 2\Re_1 A_0 \sin(n\omega_{\mathrm{LO}}t + n\theta_{\mathrm{LO}}) \\ -A_{-1}(\Re_1+\Re_2)\sin(\omega_{\mathrm{IF}}t + \theta_{\mathrm{IF}} + n\omega_{\mathrm{LO}}t + n\theta_{\mathrm{LO}})] \text{ when } \Re_1 \approx \Re_2 \end{cases}. \quad \textbf{(4)}$$

For the positive frequency shift condition at the AOM, $A_1 \gg A_0$, $A_1 \gg A_{-1}$. As can be seen, by using BPDs having approximately equal responsivities (i.e., $\Re_1 \approx \Re_2$), the USB and LSB RF signals are output from the two ports of the 90° electrical hybrid [i.e., $i_1(t)$ and $i_2(t)$], respectively. For the optical CS-SSB modulation at the AOM, the optical sideband suppression ratio is expressed as $\mu_{1,-1} = (A_1/A_{-1})^2$, while the optical carrier extinction ratio is expressed as $\mu_{1,0} = (A_1/A_0)^2$. For both the USB and LSB up-converted RF signals, the sideband suppression ratio μ_{Side} and the LO leakage suppression ratio μ_{LO} can be calculated as follows:

$$\begin{cases} \mu_{\mathrm{Side}} = 10\log(\mu_{1,-1}) \quad \text{when } \Re_1 \approx \Re_2 \\ \mu_{\mathrm{LO}} = 10\log(\mu_{1,0}) \quad \text{when } \Re_1 \approx \Re_2 \end{cases}. \quad \textbf{(5)}$$

As can be seen, the LO leakage and undesired sideband suppression ratios with the up-converted RF signals are mainly determined by the optical modulation performance with the IF signal and not affected by the modulation format at the MZM. The high extinction ratio of the AOM guarantees the large sideband and LO leakage suppression ratios with the up-converted results. In this way, the proposed filter-free SSB up-converter will output LSB and USB up-converted RF signals simultaneously and separately, with the undesired sideband and the LO leakage highly suppressed.

3. EXPERIMENTAL RESULTS AND DISCUSSION

A proof-of-concept experiment is carried out based on the scheme shown in Fig. 1. The optical carrier with a wavelength of 1550.5 nm is generated from a LD (NKT Koheras BASIK X15). The IF signals are generated by a vector signal generator (Agilent E8267D, 250 kHz–43.5 GHz). The AOM (Gooch&Housego T-M200-0.1C2J-3-F2P) has a 200 MHz RF working center frequency and a 70 MHz RF working bandwidth. An IF power amplifier with a 2.5 W output power is allocated with the AOM to amplify the applied IF signal. The LO signal is generated by a microwave signal generator (Rohde & Schwarz SMA100B, 8 kHz–67 GHz). The MZM (Fujitsu FTM7938EZ) has a 40 GHz working bandwidth and a 3.5 V half-wave voltage. The BPDs (Finisar BPDV2050RQ) have a working bandwidth of 43 GHz, and the responsivity is 0.45 A/W. The 90° electrical hybrid (KRYTAR-3040440) has a working frequency range of 4–44 GHz. The optical signals are measured by an optical spectrum analyzer (APEX AP2040D) with a 5 MHz resolution. The electrical spectra are measured by an electrical spectrum analyzer (Keysight N9010AEXA, 10 Hz–44 GHz), and the error vector magnitude (EVM) values of the electrical signals are measured by using the digital modulation analysis module (Keysight VSA89600) in the real-time oscilloscope (Keysight DSOX93304, 80 GSa/s).

A 200 MHz single-tone IF signal is injected into the RF port of the AOM, and the output optical spectrum is shown as the red curve in Fig. 2(a), while the original optical carrier generated from the LD is shown as the blue curve. The inset gives the optical spectra in detail. As can be seen, the IF signal is successfully modulated with the optical CS-SSB modulation format, with the optical sideband suppression ratio of 80 dB, and the optical carrier extinction ratio of 72 dB, respectively. A 10 GHz LO signal is modulated at the MZM with the CS-DSB modulation format, with the optical spectrum shown in Fig. 2(b).

The electrical spectra at the two output ports of the 90° electrical hybrid are given in Figs. 3(a) and 3(b), respectively. It can be seen that the LSB and USB up-converted RF signals are output simultaneously and separately. In addition, for the frequency range of 0–34 GHz, the mixing spurs are all effectively suppressed. The high-order mixing spurs near 20 GHz are mainly composed of the frequency components at $2\omega_{\mathrm{LO}}$ and $2\omega_{\mathrm{LO}} \pm \omega_{\mathrm{IF}}$. The suppression ratios of these high-order mixing spurs are higher than 58 dB. The electrical spectra in detail are shown in the insets. For the LSB RF signal, the LO leakage suppression ratio and undesired sideband suppression ratio are 68.4 and 69.5 dB, respectively. Meanwhile, for the USB RF signal, the LO leakage and undesired sideband suppression ratios are 69.2 and 70.2 dB, respectively. The effective suppression with the mixing spurs is achieved with both the USB and the LSB up-converted results.

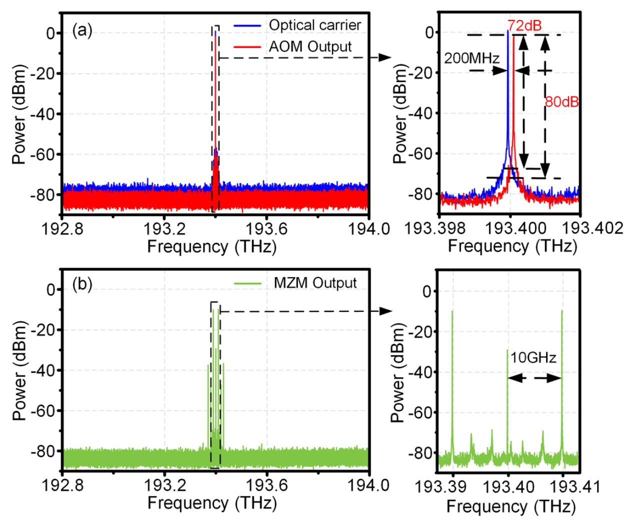

Fig. 2. Optical spectra of (a) the original optical carrier (the blue curve) and the AOM output (the red curve), (b) the MZM output (the green curve).

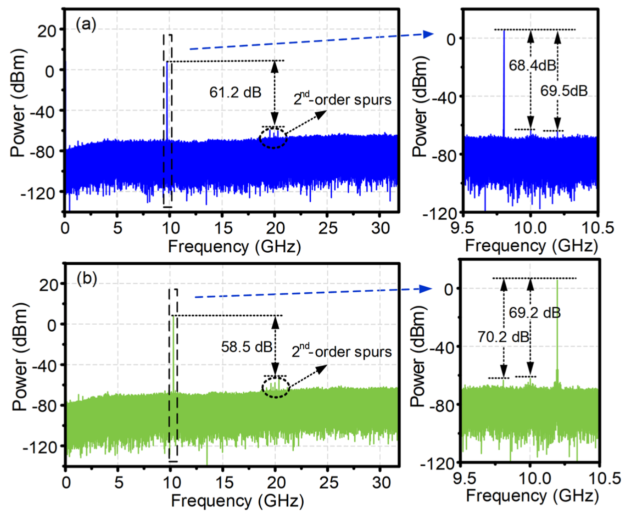

Fig. 3. Electrical spectra of the outputs from (a) one port and (b) the other port of the 90° electrical hybrid with a 200 MHz IF signal and a 10 GHz LO signal.

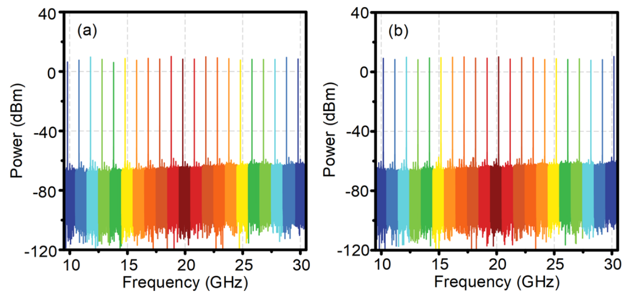

Fig. 4. Electrical spectra of the (a) LSB and (b) USB up-converted RF signals when applying a 200 MHz IF signal and tuning the LO frequency from 10–30 GHz with a step of 1 GHz.

By tuning the applied LO frequency from 10 to 30 GHz with a 1 GHz step, the electrical spectra of the LSB and USB up-converted RF signals output from the two ports of the 90° electrical hybrid are shown in Figs. 4(a) and 4(b), respectively. The corresponding LO leakage suppression ratio and the sideband suppression ratio performance are shown in Fig. 5. For the LSB up-converted results, the LO leakage suppression ratio has a mean value of 68.3 dB with a 2.3 dB fluctuation range for the whole tuning range. The sideband suppression ratio has a mean value of 70.7 dB with a 2.4 dB fluctuation range. For the USB up-converted results, the mean value of 68.5 dB with the fluctuation range of 2.8 dB is obtained for the LO leakage suppression ratio, while the sideband suppression ratio has a mean value of 70.0 dB and a fluctuation range of 2.9 dB.

Based on Eq. (5), together with the experimentally obtained optical carrier extinction ratio (72 dB) and the optical sideband suppression ratio (80 dB) shown in Fig. 2(a), the theoretical LO leakage and undesired sideband suppression ratio values are calculated to be 72 and 80 dB, respectively. Thus, the experimental results agree well with the theoretical analyses. The obtained sideband suppression ratios do not achieve the calculated value of 80 dB, which is mainly due to the amplitude and phase imbalance introduced by the used devices in the experiment.

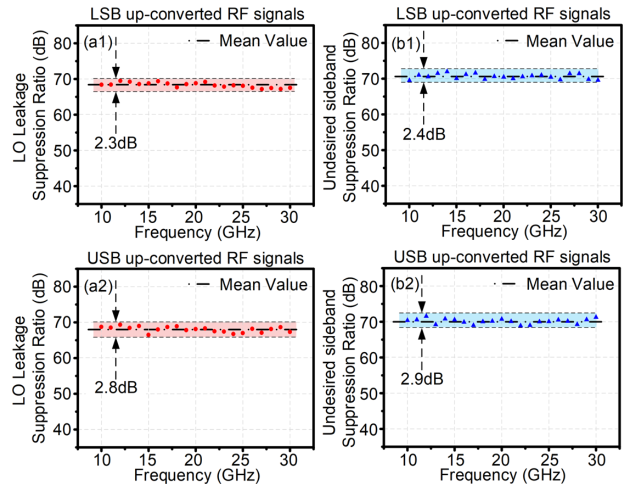

Fig. 5. (a) LO leakage suppression ratios and (b) the undesired sideband suppression ratios for the (1) LSB and (2) USB up-converted RF signals when applying a 200 MHz IF signal and tuning the LO frequency from 10–30 GHz with a step of 1 GHz.

The reliability of the proposed system is also investigated. The 128 quadrature amplitude modulation (QAM) signals centered at 200 MHz with 70 Mb/s data rates are used as the IF signals and applied to the AOM. The EVM of the applied 128-QAM IF signal is measured to be 0.89%. By tuning the LO frequency from 10 to 30 GHz with a step of 2 GHz, the measured EVM values of the LSB and USB up-converted RF signals are shown in Figs. 6(a) and 6(b), respectively. For the whole working frequency range, the EVM values for the LSB up-converted RF signals are between 1.55% and 1.86%, while those for the USB up-converted RF signals are between 1.55% and 1.88%. The EVM deterioration of less than 1% is achieved with the proposed dual-output microwave photonic SSB up-converter. Figure 6(c) gives the constellation diagrams of the original 128-QAM IF signal. As a comparison, when the LO signal is 16 and 26 GHz, the constellation diagrams of the LSB and USB up-converted RF signals are shown in Figs. 6(d)–6(g), respectively. The good performance of the dual-output microwave photonic SSB up-converter is proved.

The spurious-free dynamic range (SFDR) performance is also experimentally investigated. Two-tone IF signals with frequencies of 195 and 205 MHz are applied. The LO frequency is set to be 10 GHz. For the LSB up-conversion condition, when the IF signal power values are 5 and 10 dBm, respectively, the fundamental to third-order intermodulation distortion (IMD3) ratios are 80.8 and 69.4 dB, with the electrical spectra shown in Figs. 7(a1) and 7(a2), respectively. While for the USB up-conversion condition, the fundamental to IMD3 ratios are 80.6 and 70.3 dB, as shown in Figs. 7(b1) and 7(b2), respectively. The SFDR performances for both the LSB and USB up-conversion conditions are measured by varying the applied IF signal power, with the results shown in Figs. 7(c) and 7(d), respectively. The noise floor is measured to be -121 dBm/Hz in our experiment [22] due to the relative intensity noise (RIN) of the LD and the noise introduced by the IF amplifier allocated with the AOM. The SFDRs are measured to be 95.8 and 95.6 $\mathrm{dBc} \cdot \mathrm{Hz}^{2/3}$ for the LSB and USB up-conversion conditions, respectively. A noise floor as low as -160 dBm/Hz

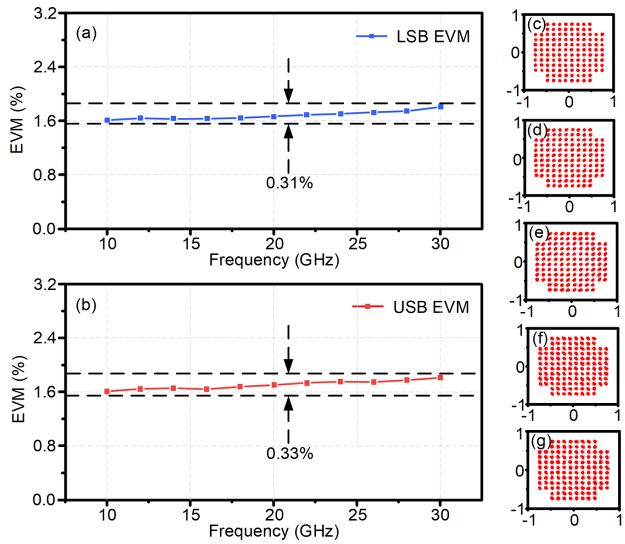

Fig. 6. EVM values of (a) the LSB and (b) the USB up-converted 128-QAM RF signals versus the LO frequency. The constellation diagrams of (c) the 128-QAM IF signal, (d) the LSB, and (e) the USB up-converted 128-QAM RF signals when applying a 16 GHz LO signal, and (f) the LSB and (g) the USB up-converted 128-QAM signals when applying a 26 GHz LO signal.

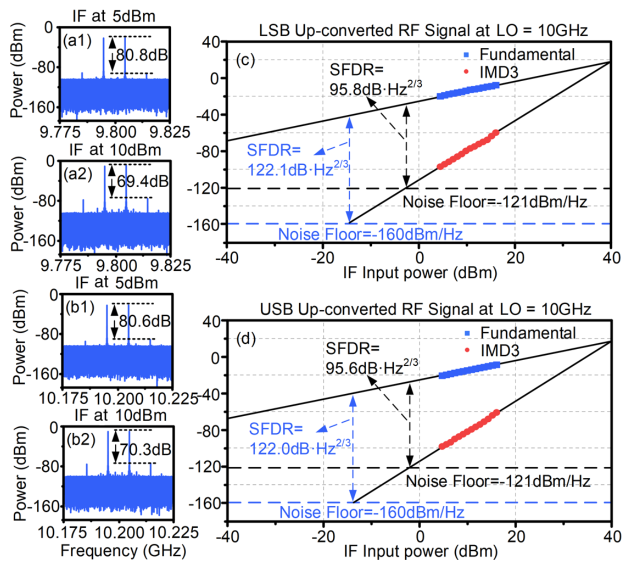

Fig. 7. Experimental electrical spectra of the output fundamental signal and the third-order intermodulation distortion (IMD3) with 1 Hz resolution bandwidth (RBW) for the (a) LSB and (b) USB up-conversion conditions when the IF signal power is set to be (1) 5 and (2) 10 dBm, respectively. Experimental SFDR performance for the (c) LSB and (d) USB up-conversion.

can be possible by using devices with high performances in the system [23]. For this condition, the SFDR can be improved to higher than 122.0 $\mathrm{dBc \cdot Hz^{2/3}}$ for both the LSB and USB up-conversion cases.

It should be noted that the instantaneous bandwidth and working frequency range of the applied IF signal are limited by the bandwidth of the AOM. For the AOM with the RF working center frequency of 200 MHz and bandwidth of 70 MHz used in our experiment, the IF working frequency range of the experimental system is 165–235 MHz. Meanwhile, the wide working frequency range of the LO signal is guaranteed by using an MZM to modulate the LO signal. Thus, this scheme can find applications in the RF systems with narrow instantaneous bandwidth and wide working frequency range, such as wireless communication and future internet of things (IoT) [24]. An IF power amplifier having a high output power is allocated with the AOM, which increases the power consumption of the scheme. With the development of integrated microwave photonics [25], the optical SSB modulation with high sideband rejection ratio can be achieved without using an AOM. The introduction of these new techniques can ease the high power consumption and extend the working frequency range of the applied IF signals of the proposed scheme.

4. CONCLUSION

In conclusion, a dual-output filter-free microwave photonic SSB up-converter is proposed and experimentally demonstrated. The LSB and USB up-converted RF signals can be output simultaneously without the filters. By using an AOM to modulate the IF signals and an MZM to modulate the LO signals, the high undesired sideband suppression ratios and LO leakage suppression ratios in a wide frequency range are achieved. The dual-output SSB up-conversion is experimentally achieved within the 10–30 GHz working frequency range. The undesired sideband and LO leakage suppression ratios are larger than 67 dB. The SFDR higher than 95.6 $\mathrm{dBc \cdot Hz^{2/3}}$ is achieved for both the LSB and USB up-conversion conditions.

Funding. National Natural Science Foundation of China (61971222); Fundamental Research Funds for the Central Universities (NC2018005, NE2017002).

Disclosures. The authors declare no conflicts of interest.

Data Availability. Data underlying the results presented in this paper are not publicly available at this time but may be obtained from the authors upon reasonable request.

REFERENCES

1. S. Koenig, D. Lopez-Diaz, and J. Antes, "Wireless sub-THz communication system with high data rate," Nat. Photonics **7**, 977–981 (2013).
2. D. Zhu and S. Pan, "Broadband cognitive radio enabled by photonics," J. Lightwave Technol. **38**, 3076–3088 (2020).
3. S. Pan and Y. Zhang, "Microwave photonic radars," J. Lightwave Technol. **38**, 5450–5484 (2020).
4. C. Kurth, "Generation of single-sideband signals in multiplex communication systems," IEEE Trans. Circuits Syst. **23**, 1–17 (1976).
5. H. Nyquist and K. W. Pfleger, "Effect of the quadrature component in single side-band transmission," Bell Syst. Tech. J. **19**, 63–73 (1940).
6. J. Lee, H. Lou, and D. Toumpakaris, "SNR analysis of OFDM systems in the presence of carrier frequency offset for fading channels," IEEE Trans. Wireless Commun. **5**, 3360–3364 (2006).
7. Y. Ye, J. Zhang, and R. Tong, "A linear resistive single sideband (SSB) up-converter for E-band wireless communication," in *IEEE International Wireless Symposium (IWS)* (2014), pp. 1–4.
8. B. C. Henderson and J. A. Cook, "Image-reject and single-sideband mixers," WJ Tech. Note **12**, 1–6 (1985).
9. M. Wang and C. E. Saavedra, "Fully monolithic single-sideband upconverter mixer with sideband selection," in *IEEE MTT-S International Microwave Symposium* (2011), pp. 1–4.
10. J. Yao, "Microwave photonics," J. Lightwave Technol. **27**, 314–335 (2009).

11. V. J. Urick, K. J. Williams, and J. D. McKinney, *Fundamentals of Microwave Photonics* (Wiley, 2015).
12. B. Yang, X. Jin, and Y. Chen, "Photonic microwave up-conversion of vector signals based on an optoelectronic oscillator," IEEE Photon. Technol. Lett. **25**, 1758–1761 (2013).
13. Y. Gao, A. Wen, W. Jiang, Y. Fan, Y. He, and D. Zhou, "Fundamental/subharmonic photonic microwave I/Q up-converter for single sideband and vector signal generation," IEEE Trans. Microwave Theory Tech. **66**, 4282–4292 (2018).
14. Y. Gao, A. Wen, W. Jiang, Y. Fan, D. Zhou, and Y. He, "Wideband photonic microwave SSB up-converter and I/Q modulator," J. Lightwave Technol. **35**, 4023–4032 (2017).
15. C. Huang, E. H. W. Chan, and C. B. Albert, "A compact photonics-based single sideband mixer without using high-frequency electrical components," IEEE Photon. J. **11**, 7204509 (2019).
16. S. H. Lee, H. J. Kim, and J. I. Song, "Broadband photonic single sideband frequency up-converter based on the cross polarization modulation effect in a semiconductor optical amplifier for radio-over-fiber systems," Opt. Express **22**, 183–192 (2014).
17. J. Li, Y. Wang, and D. Wang, "A microwave photonic mixer using a frequency-doubled local oscillator," IEEE Photon. J. **10**, 5501210 (2018).
18. Z. Tang and S. Pan, "A filter-free photonic microwave single sideband mixer," IEEE Microw. Wirel. Compon. Lett. **26**, 67–69 (2015).
19. J. Ma, A. Wen, and Z. Tu, "Filter-free photonic microwave upconverter with frequency quadrupling," Appl. Opt. **58**, 7915–7920 (2019).
20. X. Li, Y. Xu, and J. Yu, "Single-sideband W-band photonic vector millimeter-wave signal generation by one single I/Q modulator," Opt. Lett. **41**, 4162–4165 (2016).
21. H. G. de Chatellus, L. R. Cortés, and C. Schnébelin, "Reconfigurable photonic generation of broadband chirped waveforms using a single CW laser and low-frequency electronics," Nat. Commun. **9**, 2438 (2018).
22. C. Rauscher, V. Janssen, and R. Minihold, *Fundamentals of Spectrum Analysis* (Rohde & Schwarz, 2007), Chap. 5.
23. W. Loh, F. J. O'Donnell, J. J. Plant, M. A. Brattain, L. J. Missaggia, and P. W. Juodawlkis, "Packaged, high-power, narrow-linewidth slab-coupled optical waveguide external cavity laser (SCOWECL)," IEEE Photon. Technol. Lett. **23**, 974–976 (2011).
24. K. B. Letaief, W. Chen, Y. Shi, J. Zhang, and Y. J. A. Zhang, "The roadmap to 6G: AI empowered wireless networks," IEEE Commun. Mag. **57**(8), 84–90 (2019).
25. M. Tan, X. Xu, J. Wu, T. G. Nguyen, S. T. Chu, B. E. Little, and D. J. Moss, "Orthogonally polarized RF optical single sideband generation with integrated ring resonators," J. Semicond. **42**, 041305 (2021).